Physics Letters B 736 (2014) 361–364

Contents lists available at ScienceDirect

Physics Letters B

www.elsevier.com/locate/physletb

Measurements of the ^{40}Ar(n, γ)^{41}Ar radiative-capture cross section between 0.4 and 14.8 MeV

Megha Bhike [a,b,*], B. Fallin [a,b], W. Tornow [a,b]

[a] Department of Physics, Duke University, Durham, NC 27708, USA
[b] Triangle Universities Nuclear Laboratory, Durham, NC 27708, USA

ARTICLE INFO

Article history:
Received 29 April 2014
Received in revised form 23 July 2014
Accepted 23 July 2014
Available online 30 July 2014
Editor: D.F. Geesaman

Keywords:
Neutron radiative capture
Neutron induced background
Neutrino detectors
Double-beta decay detectors
Dark matter detectors

ABSTRACT

The ^{40}Ar(n, γ)^{41}Ar neutron capture cross section has been measured between 0.4 and 14.8 MeV neutron energy using the activation technique. The data are important for estimating backgrounds in argon-based neutrino and dark-matter detectors and in the neutrino-less double-beta decay search GERDA, which uses liquid argon as cooling and shielding medium. For the first time the ^{40}Ar(n, γ)^{41}Ar cross section has been measured for neutron energies above 1 MeV. Our results are compared to the evaluation ENDF/B-VII.1 and the calculated prediction TENDL-2013. The latter agrees very well with the present results.

1. Introduction

During the past few years, neutron induced reaction studies on ^{40}Ar have been the focus of intensive experimental work. The reason for these activities is based on features of liquid argon that makes it an attractive detection and shielding medium in dark matter and double-beta decay searches, respectively. Because liquid argon allows for the construction of large-scale detectors, it is also an ideal medium for the detection of accelerator and core-collapse supernova neutrinos and anti-neutrinos. For example, the detector currently designed for the **L**ong **B**aseline **N**eutrino **E**xperiment (LBNE) [1] uses liquid argon. The natural abundance of argon consists of 99.6% ^{40}Ar, with only small admixtures of ^{36}Ar (0.3%) and ^{38}Ar (0.06%). Therefore, in the following we will denote natural argon by ^{40}Ar. Although most liquid ^{40}Ar-based detectors are or will be operated deep underground to minimize cosmic-ray induced background events, spallation neutrons are a concern, because they can mimic signals which are indistinguishable from the signals of interest.

In order to better determine the importance of such background events, data for the reactions ^{40}Ar(n, n$'\gamma$)^{40}Ar [2], ^{40}Ar(n, n)^{40}Ar [3], and ^{40}Ar(n, p)^{40}Cl [4] have recently been obtained between about 5 and 30 MeV to guide evaluations and theoretical calculations aimed at covering the full energy range of interest for these neutron-induced reactions. However, data for the important ^{40}Ar(n, γ)^{41}Ar radiative-capture reaction do not exist for energies above 1 MeV. The prompt γ rays originating from the de-excitation of the daughter nucleus ^{41}Ar have energies totaling more than 6100 keV. The nucleus ^{41}Ar itself is radioactive and β decays with a ground-state to ground-state Q-value of 2491.6 keV and $T_{1/2} = 1.83$ h to ^{41}K, which in turn de-excites via γ-ray emission, as shown in Fig. 1. The β- and γ-ray radiation associated with the decay of ^{41}Ar could be a potential background in ^{40}Ar-based detection systems of rare events. For example, the GERDA Collaboration [5] uses liquid ^{40}Ar as cooling and shielding material for their HPGe detectors. The de-excitation γ rays of ^{41}Ar with energies above about 2300 keV could Compton scatter into these detectors, potentially producing a signal in the vicinity of 2039 keV, the Q-value of $0\nu\beta\beta$ decay of ^{76}Ge.

Currently, the ^{40}Ar(n, γ)^{41}Ar cross section information above 1 MeV neutron energy is solely based on the extension of evaluations and model calculations to higher energies. In view of the importance of this reaction for ongoing and planned rare event searches, the neutron radiative-capture cross section has been measured at ten energies between 0.4 and 14.8 MeV.

2. Experimental setup and procedure for argon irradiation

Monoenergetic neutrons were produced at energies between 0.4 and 3.4 MeV with the ^{3}H(p, n)^{3}He reaction, and at energies

* Corresponding author at: Department of Physics, Duke University, Durham, NC 27708, USA.
E-mail address: megha@tunl.duke.edu (M. Bhike).

http://dx.doi.org/10.1016/j.physletb.2014.07.044

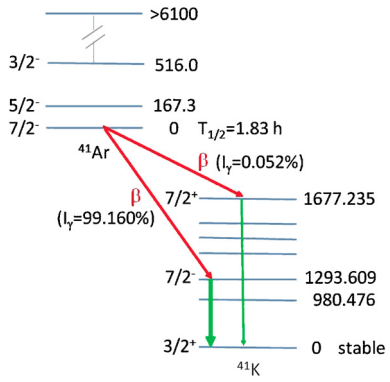

Fig. 1. (Color online) Partial level scheme of ^{41}Ar and its daughter nucleus ^{41}K. All energies are given in keV.

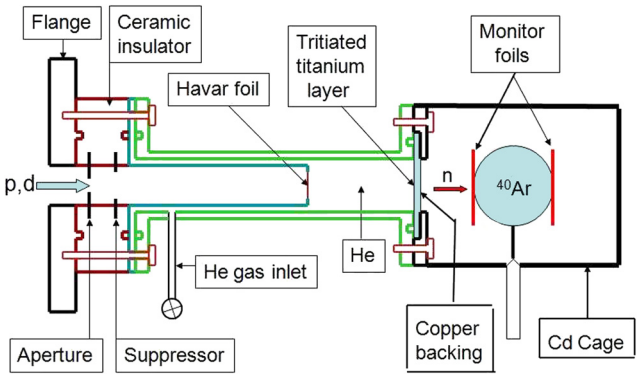

Fig. 2. (Color online) Schematic of tritiated target assembly used for neutron production via the reactions ^{2}H(d,n)^{3}He and ^{3}H(d,n)^{4}He.

between 4.1 and 7.0 MeV and at 14.8 MeV with the ^{2}H(d,n)^{3}He and ^{3}H(d,n)^{4}He reaction, respectively. The charged-particle beams were accelerated by the tandem accelerator of the Triangle Universities Nuclear Laboratory (TUNL) tandem accelerator. As shown in Fig. 2, the experimental setup used for the measurements with the ^{3}H(p,n)^{3}He reaction ($Q = -0.76$ MeV) consisted of a tritiated titanium target. An amount of 2.1 Ci of ^{3}H was loaded into a 2.2 mg/cm^2 thick layer of titanium with diameter of 16 mm. The titanium, in turn, was evaporated onto a 0.4 mm thick copper backing, which also served as proton beam stop. In order to avoid a potential tritium release into the accelerator vacuum system, a 6.5 μm thick Havar foil separated the tritiated target from the accelerator. The volume between the Havar foil and the tritiated target was filled with 1.5 atm of helium to prevent overheating of the Havar foil and the titanium layer due to the energy deposition of the incident charged-particle beam. Typical proton beam currents on target were 3.5 μA. The entire target assembly, and especially the outer surface of the copper backing, were cooled with compressed and refrigerated air to prevent overheating of the tritiated target, which could result in a release of tritium.

Once the incident proton energy exceeds about 3 MeV, corresponding to a neutron energy of greater than 2.2 MeV, the neutrons of interest are accompanied by lower-energy neutrons originating from (p,n) reactions on the titanium and its copper backing. Therefore, for the neutron energies of $E_n = 2.72$ and 3.41 MeV, auxiliary measurements were performed with an untritiated, but otherwise identical target. The tritiated and untritiated measurements were normalized to the accumulated proton charge on target.

For the measurements with the ^{2}H(d,n)^{3}He reaction ($Q = +3.27$ MeV) a 3 cm long gas cell pressurized to 3 atm of high-purity deuterium gas was used. A schematic of the deuterium gas cell used in the present experiment is given in Ref. [6]. Again, a 6.5 μm Havar foil separated the gas from the accelerator vacuum. The deuteron beam stop and the inner walls of the gas cell consisted of a 0.3 mm thick layer of tantalum. For deuteron energies above 2.23 MeV, the deuterons can break up on the entrance collimator, the Havar foil and the tantalum beam stop, resulting in lower-energy neutrons than the neutrons from the ^{2}H(d,n)^{3}He reaction of interest. Therefore, for neutron energies above $E_n = 5.5$ MeV, auxiliary measurements were performed with the deuterium gas pumped out. The charge deposited by the incident deuteron beam on the deuterium gas cell was used for normalization purposes for these two types of experiments.

The tritiated target described above and shown in Fig. 2 was also used for the ^{3}H(d,n)^{4}He reaction. In this case, the Havar foil (and the helium gas) degraded the incident deuteron energy from 2 MeV, the lowest beam energy available with the TUNL tandem accelerator, to overlap with the strong 107 keV resonance of the ^{3}H(d,n)^{4}He reaction, producing 14.8 MeV neutrons at 0°. Here, breakup neutrons are not produced due to the low incident deuteron beam energy.

Table 1
Relevant data for the reactions of interest in the present work.

Nuclear reaction	half-life	γ-ray energy (keV)	γ-ray intensity (%)
^{40}Ar(n,γ)^{41}Ar	109.61(4) m	1293.64(4)	99.16
^{115}In(n,n′)^{115m}In	4.486(4) h	335.241(25)	45.8(22)
^{115}In(n,γ)^{116m1}In	54.29(17) m	1293.56(2)	84.8(12)
^{197}Au(n,2n)^{196}Au	6.1669(6) d	355.73(5)	87

The argon gas was contained in a stainless steel sphere with inner diameter of 20 mm and wall thickness of 0.5 mm [7]. The argon mass was 1.585 g, resulting in a pressure of 210 atm inside of the sphere. The sphere was positioned at a distance of 20 mm from the end of the tritiated target or deuterium gas cell. Two neutron fluence monitor foils were attached to the sphere, as shown in Fig. 2. Indium foils of 19.05 mm diameter and 0.125 mm thickness were used, except at 14.8 MeV, where gold foils of the same diameter and 0.1 mm thickness were employed to determine the neutron fluence from the ^{197}Au(n,2n)^{196}Au reaction. At the lowest energy the ^{115}In(n,γ)^{116m1}In was used, while for the higher energies the ^{115}In(n,n′)^{115m}In reaction was preferred. See Table 1 for the relevant data for the reactions studied in the present work. The sphere-foil assembly was enclosed by a cage made of 0.5 mm thick cadmium, as shown in Fig. 2. The cadmium efficiently eliminated thermal neutrons from interacting with the argon gas and the monitor foils. Measurements with an identical, but empty stainless steel sphere, were also performed at a few energies. The irradiation time of the sphere-foil assembly was typically 2 hours at each neutron energy. The neutron flux was monitored with a BC-501A liquid scintillator [8] positioned at 0° relative to the incident charged-particle beam at a distance of 2.9 m from the neutron source. This detector has excellent neutron-gamma-ray pulse-shape discrimination properties. During irradiation, variations of the neutron flux stayed within 3% of its mean value.

3. Data analysis

After irradiation, the argon sphere and the monitor foils were transferred to TUNL's γ-ray counting facility, consisting of a five well-shielded 60% High-Purity Germanium (HPGe) detectors. The activated argon sphere was placed at a distance of 5 cm from the front face of one of the HPGe detectors. The two monitor foils were counted together, also at a distance of 5 cm from a second HPGe detector. The absolute efficiency of the HPGe detectors

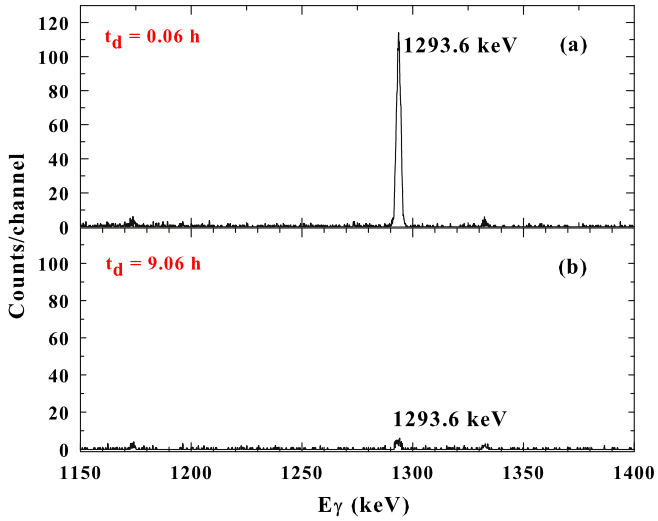

Fig. 3. (Color online) (a) ^{41}K γ-ray line at 1293.6 MeV measured for 1 hour with a HPGe detector starting 0.06 h after the 2 h irradiation time of ^{40}Ar with 4.09 MeV neutrons, (b) same as above, but with starting time of 9.06 h after irradiation.

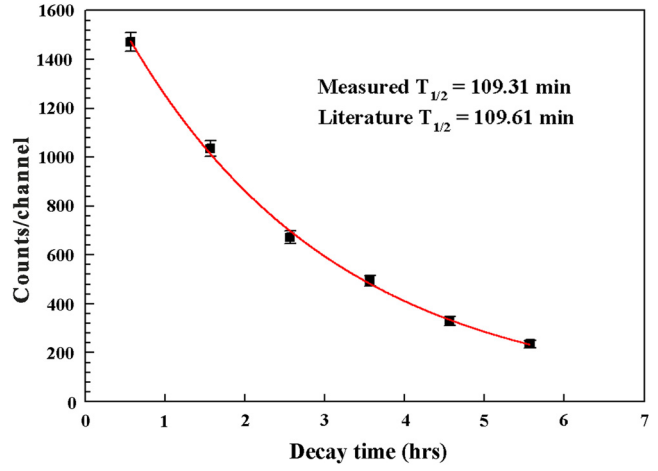

Fig. 4. (Color online) Measured decay curve of the ^{41}K 1293.6 keV activity.

was measured with calibrated γ-ray test sources. The GENIE data-acquisition system was used [9]. As can be seen in Fig. 1, the detection of the 1293.64 keV γ ray with $I_\gamma = 99.16\%$ provides an excellent opportunity for measuring the ^{40}Ar(n, γ)^{41}Ar cross section. Fig. 3 (a) shows a γ-ray spectrum displaying the 1293.64 keV line obtained at $E_n = 4.09$ MeV after an irradiation time $t_i = 2$ h and recorded for a measuring time $t_m = 1$ h starting at $t_d = 0.06$ h after the end of irradiation. Fig. 3 (b) shows the spectrum measured after $t_d = 9.06$ h, again for $t_m = 1$ h. As can be seen from Fig. 4, the decay of the γ-ray intensity was measured over a time period of typically three half-life times. The same was done for the indium monitor foils. The activity measurements of the Au foils were started about 5 days after irradiation to allow the radiation from the isomeric state of ^{196m}Au to decay away. The Au foils were counted for typically 3 days. The measurements made with the empty ^{40}Ar cell showed no background lines in the energy region of interest. Monte Carlo calculations were performed to account for the geometry difference between the calibration γ-ray sources and the ^{40}Ar sphere. Corrections for self-absorption were also made. Finally, the measured activities were corrected for the branching ratios given in Table 2.

The neutron flux was determined from the monitor foils using the activation formula [6]

Table 2
Mean neutron energy and energy spread, monitor reaction cross-section values used, and ^{40}Ar(n, γ)^{41}Ar cross-section results obtained in the present work.

Neutron energy $E_n \pm \triangle E_n$ (MeV)	Monitor reactions σ (mb)	^{40}Ar(n, γ)^{41}Ar σ (mb)
0.37 ± 0.10	180.00 ± 5.40	1.19 ± 0.06
1.31 ± 0.10	132.20 ± 3.17	1.03 ± 0.07
1.84 ± 0.13	236.74 ± 5.68	0.75 ± 0.05
2.72 ± 0.16	344.65 ± 8.09	0.64 ± 0.10
3.41 ± 0.16	335.76 ± 7.89	0.57 ± 0.10
4.09 ± 0.63	318.48 ± 7.48	0.48 ± 0.03
5.46 ± 0.47	337.95 ± 8.79	0.37 ± 0.05
6.00 ± 0.41	348.59 ± 9.06	0.36 ± 0.06
7.04 ± 0.34	328.51 ± 11.66	0.31 ± 0.05
14.80 ± 0.07	2164.20 ± 23.37	0.45 ± 0.02

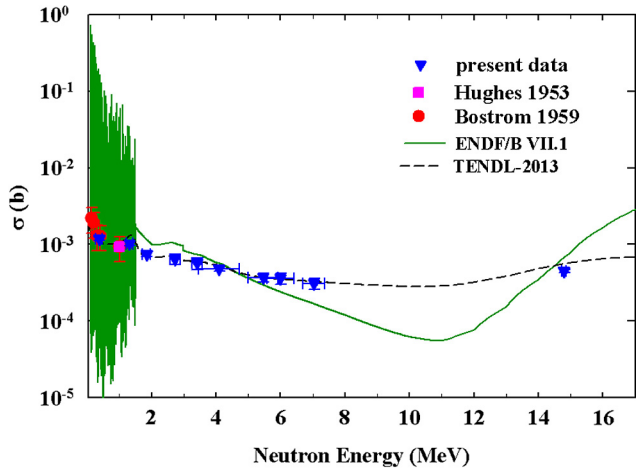

Fig. 5. (Color online) Results for ^{40}Ar(n, γ)^{41}Ar radiative-capture cross section obtained in the present work (triangles) in comparison to the ENDF/B VII.1 evaluation (solid curve and shaded area below 1.5 MeV) and the TENDL-2013 prediction (dashed curve). The previous data below 1 MeV of Hughes (square) [15] and Bostrom et al. (circle) [16] are also shown.

$$\phi_n = \frac{A_m \lambda_m}{N_m \sigma_m \epsilon_m I_{\gamma_m} (1 - e^{-\lambda_m t_i}) e^{-\lambda_m t_d} (1 - e^{-\lambda_m t_m})}, \quad (1)$$

where the induced activity A_m is the total yield in the photopeak, N_m is the total number of target nuclei, ϕ_n is the neutron flux per square centimeter and second obtained from the monitor reaction, λ_m is the decay constant of the residual nucleus, ϵ_m is the photopeak efficiency for the γ-ray energy of interest, I_{γ_m} is its branching ratio, t_i is the irradiation time, t_d is the decay time between the end of irradiation and the begin of off-line counting, and t_m is the measuring time. The cross-section values for the monitor reactions were taken from [10] and [11] for ^{115}In and from [12] for ^{197}Au. Because of the finite geometry of the experimental setup shown on Fig. 2, the average of the neutron fluences obtained from the two monitor foils is not identical to the neutron fluence seen by the ^{40}Ar gas. Monte Carlo calculations were performed to obtain the associated correction factors. Here, the differential cross sections of the neutron production reactions [13,14], and the attenuation in materials between the neutron production site and the points of interest in either the ^{40}Ar sphere or the downstream monitor foil were taken into account. The Monte Carlo calculations also provided the mean neutron energy and its associated energy spread, as seen by the ^{40}Ar gas.

Once the neutron flux was determined, the activation formula [6] was used again, this time solved for ^{40}Ar to extract the ^{40}Ar(n, γ)^{41}Ar cross section from the measured activity of the

Table 3
Uncertainty budget for ^{40}Ar(n, γ)^{41}Ar and monitor reaction cross-section values.

Uncertainty	Ar (%)	Monitors (%)
Counting statistics	0.2–10	0.8–11
Reference cross sections		1–4
Detector efficiency	1.5–2.5	0.7–4.5
Source geometry and self-absorption of γ-rays	1.6–1.8	0.6–6
Half-life	<0.1	<0.1
γ-ray intensity	–	<5
Neutron flux fluctuation	<1	<1
Lower-energy neutrons	<10	<10

1293.64 keV γ-ray line, and the neutron flux ϕ_n determined from the monitor foils with the equivalent quantities used in Eq. (1).

$$\sigma_{Ar} = \frac{A_{\mathrm{Ar}}\lambda_{\mathrm{Ar}}}{N_{\mathrm{Ar}}\phi_n\epsilon_{\mathrm{Ar}}I_{\gamma\mathrm{Ar}}(1-e^{-\lambda_{\mathrm{Ar}}t_i})e^{-\lambda_{\mathrm{Ar}}t_d}(1-e^{-\lambda_{\mathrm{Ar}}t_m})} \quad (2)$$

4. Results and conclusion

The present data are shown in Fig. 5 as upside-down triangles in comparison to the previous data of Hughes et al. [15] and Bostrom et al. [16], which are limited to energies of 1 MeV and below. Very good agreement is found within the quoted uncertainties. Previous data do not exist at higher energies. Table 2 summarizes our results. The 1st column gives the mean neutron energy and its associated energy spread. The 2nd column provides the cross-section values used for the monitor reactions, and finally, the 3rd column lists the ^{40}Ar(n, γ)^{41}Ar radiative-capture cross-section results obtained in the present work. Throughout the energy range investigated, the cross section is of the order of 1 mb or below. For completeness, Table 3 gives the uncertainty budget. As can be seen, the uncertainty of the present data is governed by counting statistics, followed by the uncertainties associated with γ-ray detection efficiency. The correction for the contribution of lower-energy neutrons is largest at $E_n = 2.72$ MeV and 3.41 MeV. The individual uncertainties were added in quadrature to obtain the final uncertainties given.

The solid curve in Fig. 5, including the shaded area below 1.5 MeV, represents the prediction of the ENDF/B VII.1 evaluation [17], which slightly overestimates our data at 2 and 14.8 MeV, and slightly underestimates our data at 7.0 MeV. Surprisingly, the TENDL-2013 prediction (dashed curve) based on the TALYS code [18], is in perfect agreement with the present data. At around 11 MeV there is an almost one order of magnitude difference between the ENDF/B VII.1 evaluation and the TENDL-2013 calculation. Unfortunately, the neutron energy range between 8 and 14 MeV is not directly accessible for neutron capture experiments with current experimental techniques and procedures.

In summary, accurate data for the ^{40}Ar(n, γ)^{41}Ar radiative-capture cross section have been measured in the neutron energy range between 0.4 and 14.8 MeV. The measurements are the first reported for energies above 1 MeV and they show that the TENDL-2013 calculation gives an excellent representation of the present data in the energy range studied in the present work. This gives confidence into model calculations using TENDL-2013 for neutron capture events in ^{40}Ar-based detectors searching for rare events. One can also turn the argument around and use the TENDL-2013 calculations to obtain information on the integrated neutron flux at the site of the detector, for example at SNO [19] using the liquid argon detector DEAP/CLEAN [20] with its excellent energy resolution and pulse-shape discrimination properties.

Acknowledgements

Anton Tonchev provided valuable contributions to this work. We thank René Reifarth for providing the high-pressure spheres and the associated filling mechanism. Help from Matthew Gooden and Sean Finch is also acknowledged. This work was supported partially by the U.S. Department of Energy, Office of Nuclear Physics, under Grant No. DE-FG02-97ER41033.

References

[1] http://lbne.fnal.gov/.
[2] S. MacMullin, et al., Phys. Rev. C, Nucl. Phys. 85 (2012) 064614.
[3] S. MacMullin, M. Kidd, R. Henning, W. Tornow, C.R. Howell, M. Brown, Phys. Rev. C, Nucl. Phys. 87 (2013) 054613.
[4] C. Bhatia, S.W. Finch, M.E. Gooden, W. Tornow, Phys. Rev. C, Nucl. Phys. 86 (2012) 041602(R).
[5] M. Agostini, et al., Phys. Rev. Lett. 111 (2013) 122503.
[6] M. Bhike, W. Tornow, Phys. Rev. C, Nucl. Phys. 89 (2014) 031602(R).
[7] G. Rupp, D. Petrich, F. Käppeler, J. Kaltenbaek, B. Leugers, R. Reifarth, Nucl. Instrum. Methods Phys. Res., Sect. A, Accel. Spectrom. Detect. Assoc. Equip. 608 (2009) 152.
[8] http://www.detectors.saint-gobain.com.
[9] http://www.canberra.com.
[10] A.E. Johnsrud, M.G. Silbert, H.H. Barschall, Phys. Rev. 116 (1959) 927.
[11] A.B. Smith, S. Chiba, D.L. Smith, J.W. Meadows, P.T. Guenther, R.D. Lawson, R.J. Howerton, ANL/NDM-115 (1990).
[12] K.I. Zolotarev, et al., INDC(NDS)-526 (2008).
[13] H. Liskien, A. Paulsen, At. Data Nucl. Data Tables 11 (1973) 569.
[14] M. Drosg, DROSG-2000, PC database for 56 neutron source reactions, documented in the IAEA report IAEA-NDS-87 Rev. 5 (January 2000).
[15] D.J. Hughes, Phys. Rev. 91 (1953) 1423.
[16] N.A. Bostrom, I.L. Morgan, J.T. Prud'homme, P.L. Okhuyaen, O.M. Hudson Jr., Wright Air Development Centre Report TN-59-107, USA, 1959.
[17] M.B. Chadwick, et al., Nucl. Data Sheets 112 (2011) 2887.
[18] A.J. Koning, D. Rochman, Nucl. Data Sheets 113 (2012) 2841.
[19] http://www.sno.phy.queensu.ca/.
[20] http://deapclean.org/.